University of Baghdad
College of Engineering
JOURNAL OF ENGINEERING

Journal of Engineering

journal homepage: www.jcoeng.edu.iq

Volume 32 Number 11 November 2026

GIS-Based Landslide Susceptibility Mapping Using the Analytic Hierarchy Process (AHP) in Batang Kali, Selangor, Malaysia

Al-Itbi Marwa Sultan Abd[1,*], **Siti Nur Aliaa Roslan**[1], **Helmi Zulhaidi Mohd Shafri**[1,2]

[1] Department of Civil Engineering, Faculty of Engineering, Universiti Putra Malaysia (UPM), Serdang, 43400, Malaysia

[2] Geospatial Information Science Research Centre (GISRC), Faculty of Engineering, Universiti Putra Malaysia (UPM), Serdang, 43400, Malaysia

ABSTRACT

Landslides are a prevalent environmental risk in Malaysia, occurring mainly in hilly and tropical locations, often during the optimum time for heavy downpours. This study aims to assess the landslide susceptibility in Batang Kali, Selangor, Malaysia, utilizing the Analytic Hierarchy Process (AHP) based on Geographic Information Systems (GIS). Based on historical records, aerial image interpretation, and remote sensing data, in combination with field verification, a landslide database of 46 identified landslide locations was produced. Sixteen influential factors, including various topographic, hydrological, environmental, and human factors, were selected for landslide susceptibility modeling. The landslide susceptibility map was created using weighted overlay analysis and classified into five levels of susceptibility, ranging from very low to very high. The resulting susceptibility map shows that 14.68% of the study area belongs to the very low susceptibility class, while 25.84%, 20.20%, 24.90%, and 14.38% belong to low, moderate, high, and very high susceptibility classes, respectively. The susceptibility map obtained from this study serves as a realistic decision-support tool for reducing landslide risk, designing infrastructure, and promoting sustainable land management in sensitive mountainous areas. Receiver Operating Characteristic (ROC) curve analysis was performed to measure the model's predictive performance, using the Area Under the Curve (AUC) as an overall measure of model discrimination. The ROC–AUC analysis showed an AUC value of 0.722 (72.2%), indicating acceptable model performance.

Keywords: Analytic Hierarchy Process (AHP), Area Under the Curve (AUC), GIS, Landslide susceptibility mapping, Remote sensing.

1. INTRODUCTION

Landslides are among the disastrous hazards of the geomorphological environment, causing many casualties as well as damage to infrastructure and environmental degradation,

*Corresponding author
Peer review under the responsibility of University of Baghdad.
https://doi.org/10.31026/j.eng.2026.11.12
This is an open access article under the CC BY 4 license (http://creativecommons.org/licenses/by/4.0/).
Article received: 16/06/2026
Article revised: 27/09/2026
Article accepted: 25/10/2026
Article published: 01/11/2026

especially in mountainous and rapidly enlarging urbanized areas. More specifically, landslides can cause major destruction to property, farmland, and infrastructure **(Dai et al., 2025)**. Under the influence of gravity, landslides are natural and sometimes hazardous phenomena by which rocks, debris, or landslopes move down hillslopes. Landslides are a combination of slope geometry, soil and rock properties, as well as surface and groundwater processes. An example of a natural disaster that is threatening human life and property is landslides. As cities urbanize and the population in urban areas continues to grow, it expands into mountainous areas **(Woldesenbet et al., 2023)**. Climate change will exacerbate the landslide phenomenon, especially in mountainous areas, due to human activities such as increasing urbanization, deforestation, and loss of natural vegetation coverage. With such a huge number of studies on landslides, researchers, planners, and decision-makers must recognize the factors behind landslide areas all around to mitigate the harm after a fiasco brought about by the landslide **(Sharma et al., 2024).** This boils down to two aspects: the data and the methods used **(Pawar and Sharma, 2025)**. Recent studies have highlighted the need to consider a variety of environmental and human factors in the assessment of landslide susceptibility .For example, **(Dai et al., 2025)** explained that the geological, environmental, social, and economic factors change spatially and in turn affect the susceptibility and risk of landslides. Some areas have a higher risk of landslides because of the presence of roads and rivers. The findings underscore the need for the incorporation of multiple, interacting influencing factors in the construction of landslide susceptibility models.

Landslide occurrence is driven by diverse and interacting environmental and human factors, and risk assessment is fundamental to effective risk management. They are governed by a multitude of natural driving forces such as heavy precipitation, earthquakes, variations in the water level (reserves) within mountains, volcanic activity, and rapid melt of snowpack **(Xian and Wei, 2025)**. Several studies have shown the effect of geology on the occurrence of landslides **(Qiu and Wei, 2025).** According to **(Mohd Noh et al., 2024)**, the landslide at Batang Kali on December 16, 2022, was affected by geological and hydrogeological circumstances, such as clay deposits at the foot of the slope and the groundwater system. Their study also pointed out the importance of geological and subsurface factors in understanding the causes of landslides in the region. In this respect, **(Reichenbach et al., 2018)** identified 596 unique conditioning variables across 565 articles published between 1983 and 2016; this shows the variety of factors that are used in landslide susceptibility modeling. However, this multiplicity of factors also raises an important question about which factors are most appropriate for a specific study area and how to represent the combined influence of these factors in modeling landslide susceptibility.

Land use and land cover are important environmental factors in slope stability assessment and landslide susceptibility evaluation. Land cover is what is on the surface of the Earth. That encompasses everything from natural materials (plants, water [probably landform], exposed rock, and bare ground) to human-modified surfaces. Land use, in contrast, is the human use and management of land for economic and development purposes. These factors directly influence the mechanical characteristics of soil and its hydrological response to rainfall. These changes may, in turn, affect vegetation cover and land use, and vegetation cover is considered one of the key factors improving slope stability through limiting soil erosion, encouraging root reinforcement, and regulating soil moisture status **(Kozák and Šilhán, 2023)**Human activities such as deforestation, road construction, cut-and-fill slope excavation, and urban sprawl on hillsides can seriously jeopardize slope stability through

increasing landslide susceptibility at the local scale. Recent studies have further shown the relevance of land use and land cover in explaining the geographical distribution of landslides, stressing the need to add these factors to landslide susceptibility assessments **(Liu et al., 2025)**. However, the importance of land use/land cover may vary between study areas due to local environmental and human conditions, which necessitates the need for area-specific assessment of these factors in landslide susceptibility modeling.

Landslide inventory maps, because they provide fundamental information about the spatial distribution and magnitude of prehistoric slope failures, constitute some of the important components that are integrated into landslide susceptibility assessment. These inventories provide the groundwork for vulnerability, threat, and risk evaluations; they allow recognition of landslide-prone locations and a better understanding of landslide occurrence patterns **(Sujatha and Sudharsan, 2024)**. Additionally, landslide inventories reflect the legacy of the landscape and geomorphological responses to recurring deep-seated slope failure **(Kashyap and Behera, 2023)**. Furthermore, recent studies have demonstrated that the quality and completeness of landslide inventories can considerably impact the accuracy of landslide susceptibility assessments, underscoring the necessity of reliable inventory data for landslide susceptibility modeling **(Lv et al., 2024)**. However, the completeness and spatial accuracy of the landslide inventories still pose a challenge, especially in mountainous areas with dense vegetation where some landslides may be difficult to detect and map. Thus, accurate monitoring of landslides and their susceptibility is critical for disaster risk reduction, hazard mitigation planning, and an effective landslide management system.

The power of RS technology to provide information over large spatial scales makes it an essential tool for landslide detection, monitoring, and susceptibility assessment. This is made especially difficult in tropical environments, where details of terrain or features are obscured by dense vegetation, and identification of specific landslide-related landforms is challenging. So, the accuracy of landslide inventory maps generated for these areas tends to be lower than in temperate countries. Recent studies have shown the potential of remote sensing data for the improvement of landslide monitoring and assessment of their probability of occurrence in locations where field surveys are not easy to carry out. **(Liu et al., 2025)** showed that the combination of remote sensing and geographic information systems (GIS) with different environmental parameters can assist in identifying the geographical variability of landslide occurrence and increase the understanding of the factors that influence them. In addition to data quality, landslide susceptibility models are highly reliant on suitable conditioning factor selection, as the use of irrelevant variables can lead to reduced model performance. However, there is no universal set of configuration factors for landslide susceptibility modeling, as the importance and contribution of each factor vary according to the local environmental, climatic, geological, and human conditions. Hence, the selection of appropriate configuration factors remains a key challenge for the development of reliable models of landslide susceptibility. Accordingly, in this study, satellite-derived data and several landslide conditioning factors were integrated using geospatial approaches toward enhanced landslide susceptibility estimation and effective hazard monitoring over the study area.

Mapping of landslide susceptibility has been done in several studies using GIS and machine learning approaches. Nevertheless, the implementation of the GIS-based Analytic Hierarchy Process (GIS-AHP) for the assessment of landslide susceptibility in Batang Kali area, particularly after the landslide tragedy in 2022, is still somewhat scarce. Moreover, the integrated evaluation of topographic, hydrological, environmental, and human aspects using

the GIS-AHP approach has not been given enough consideration in this region. Therefore, this study evaluates landslide susceptibility of the landslides in Batang Kali, Selangor, Malaysia, by utilizing sixteen influencing factors and a GIS-AHP approach. The generated susceptibility map is evaluated using ROC-AUC analysis for its predictive performance.

2. MATERIALS AND METHODS

2.1 The Study Area

The area of study in this paper was selected as Batang Kali, Hulu Selangor District, Selangor, Malaysia due to its high landslide hazard and exposure risk from recreation and development activities as shown in **Fig. 1**. The area is situated approximately 50 km northeast of Kuala Lumpur and possesses a partially agricultural land-use matrix (approximately 75%) followed by residential development (approximately 20%). Other such areas include forest reserves, private estates, and urban developments. Batang Kali is among the most recognized ecotourism sites with outdoor recreational activities such as hiking, trekking and glamping that could heighten human exposure to slope-related hazards **(Mohd Noh et al., 2024).**

It has a tropical climate and slight seasonal temperature differences. The temperature is almost always warm, and the relative humidity is high year-round. Annual rainfall exceeds 2,700 mm and occurs there in most months of the year, except under slightly dry conditions between June and July. Wind conditions are light to moderate, generally from the southwest. Seasonality can be altered by regional atmospheric circulation dynamics during monsoons **(Ishak et al., 2025).**

Main Series granites, metamorphic rocks, and colluvial deposits underline the site and immediately adjacent land. Metamorphic rocks, which include interleaved layers of schist and phyllite, form the oldest rock types. Biotite porphyry granite is the representative of the main series granite. The boundary between the two basement layers is in the middle of the study region. The surface sediments covering the two basement units of the valley are colluvium deposits. The most pronounced features of faulting and tectonic activity in the region are included in the granite and metamorphic bedrock. Batang Kali is prone to landslides because it is close to the foot of the tectonically active Titiwangsa Range **(Selamat et al., 2023).**

3. METHODOLOGY

3.1 Landslide Inventory Map

Landslide inventory maps are a prerequisite input for landslide susceptibility assessment, since they include geographic information on the extent of past slope failure events. The landslide inventory dataset, compiling 46 locations of historical landslides used in this study, was taken from previous studies and historical records **(Chen et al., 2025)**. These 46 identified landslide locations were used as a landslide inventory dataset for susceptibility analysis and as reference landslide locations to assess the spatial relationship between the observed landslide events and influencing factors included in the GIS-AHP model. Particular focus was placed on the catastrophic landslide event that occurred at Batang Kali on 16 December 2022, which devastated agricultural land and camping grounds in Hulu Selangor **(Petley, 2023)**, alongside information from the Department of Minerals and Geosciences Malaysia and the Department of Survey and Mapping Malaysia, as shown in **Fig. 2**.

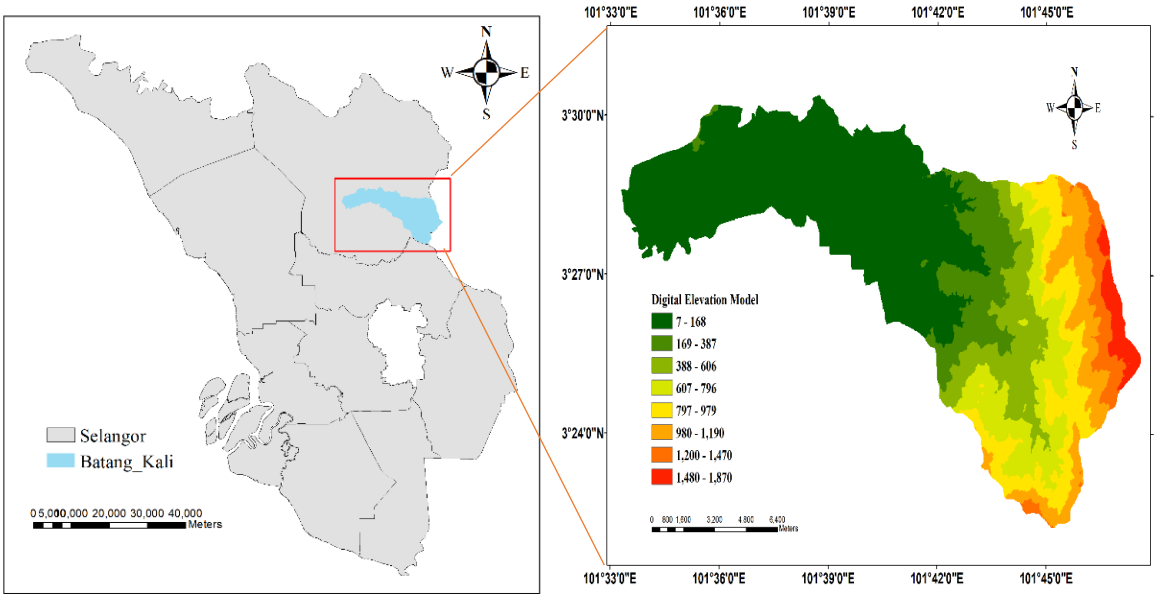


Figure 1. Location of Batang Kali, Selangor, Malaysia

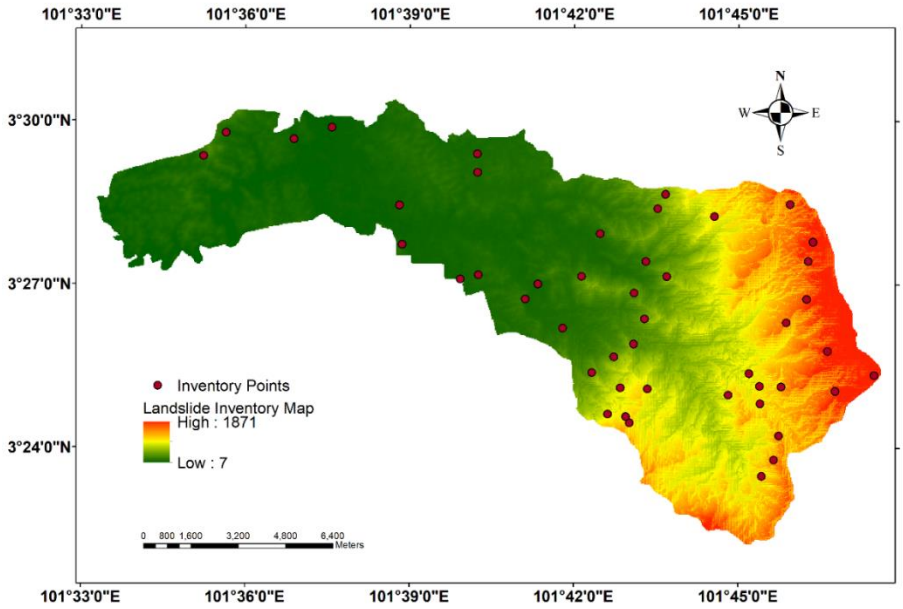


Figure 2. The landslide inventory map for the study area displays the distribution of landslides.

3.2 Layers of Landslide-Influencing Information

Study area preparation for spatial data and landslide susceptibility analysis using ArcGIS 10 and Google Earth Pro. A predictive model was developed by combining sixteen influencing factors associated with landslide occurrence, which were extracted and integrated into a GIS environment, providing a reliable methodology for susceptibility assessment. These variables comprise topographic (such as slope, aspect, curvature, and altitude), hydrological (including TWI, TRI, STI, SPI), environmental factors (like distance to lineaments and rivers),

and anthropogenic characteristics such as rainfall, LULC, NDVI, NDBI, and SMI. Concerning the landslide susceptibility modeling, all the thematic layers were normalized and converted into an appropriate GIS format (raster) for spatial analysis, and their association with historically reported landslide occurrences was evaluated.
The selection of the sixteen predictors was based both on reliable spatial data available for the study area and their established influence on landslide occurrence in previous studies. The influencing factors did not include soil and lithology/geology maps, due to the difficulties in getting acceptable spatial datasets with adequate coverage and accuracy from Malaysian data sources for the study area. Instead, the distance from the lineaments was included to represent an important feature of the structural geological conditions that may affect slope instability. However, a limitation of the study is the lack of precise information about the soil and lithology/geology, as such factors affect soil strength, permeability, weather, and groundwater conditions and hence the susceptibility to landslides.

3.2.1 Slope

Slope angle is more correlated to landslide susceptibility, and increased shear forces are seen on steeper slopes **(Adhikari and Dhakal, 2026)**. Available sliding soil is often drastically reduced on steep slopes (>25 degrees) **(Abdo, 2025)**. As shown in **Fig. 3a**, the present study slope map was extracted from the DEM and classified into 5 classes: 0–10°, 10–20°, 20–30°, 30–40°, and >40°, which are defined according to the definition. **Fig. 3a**, proportions of historical landslide event distribution analysis reveal (20°to 40°slope angles), where 86.95% of landslides are observed in this sector **(Table 4)**.

3.2.2 Aspect

The impact on hydrological processes, in turn, affects transpiration and evaporation. Accordingly, root development, vegetation cover, and soil weathering on slopes are regulated by hydrological processes in arid regions **(Zhou et al., 2023)**. Certain factors, including sunshine (drying the soil), winds, rainfall (degree of saturation in the presence of water), and flow interruptions (conductive to landsliding due to lack of support), are a function of slope direction **(Al'Afif et al., 2024)**. In this study, the aspect map was developed from digital elevation model (DEM) under 10 classes: Flat (-1) North (0-22.5) North East (22.5-67.5) East (67.5-112.5) South East (112.5-157.5) South (157.5-202.5) South West (202.5-247.5) West (247.5-292.5) North West (292.5-337.5) North (337.5-360) as shown in **Fig. 3b**. A spatial distribution study found that 32.61% of landslides occurred on northwest-facing slopes, followed by 28.26% on west-facing slopes and 26.08% on north-facing slopes (337.5–360°). The remaining landslides were distributed across the northeast, southwest, and north (0–22.5°) aspects, each accounting for 4.35%, while no landslides were recorded on flat, east-, southeast-, or south-facing slopes **(Table 4)**.

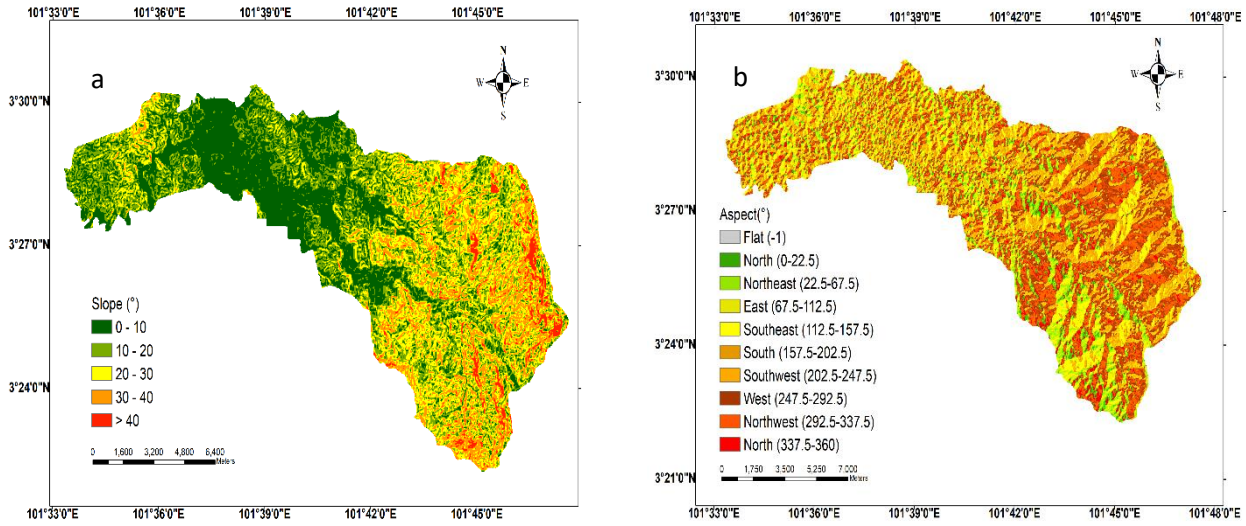
3.2.3 Curvature

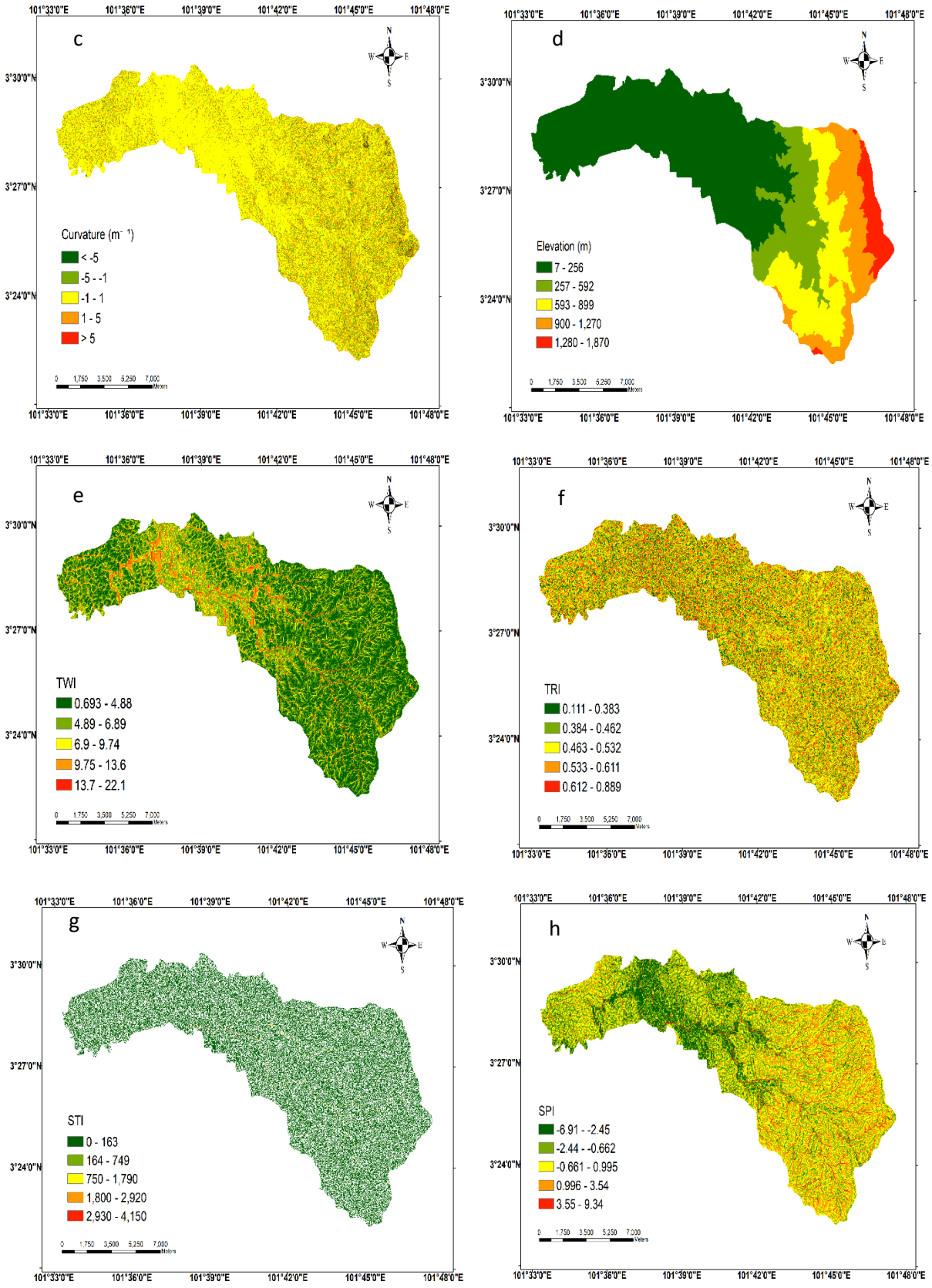
Curvature maps show whether the slope is convex or concave, which shows how far off a surface is from being flat **(Addis et al., 2024)**. Concavity (Convex vs. concave) and slope describe the curvature of the terrain prospected, where positive indicates a surface that contains convex or hollows, while negative supports concave or noses, forcing a direct relation with pixel concavity, which denotes zero orientation over a straight surface without any slope. These three types of slope morphologies greatly influence slope instabilities by

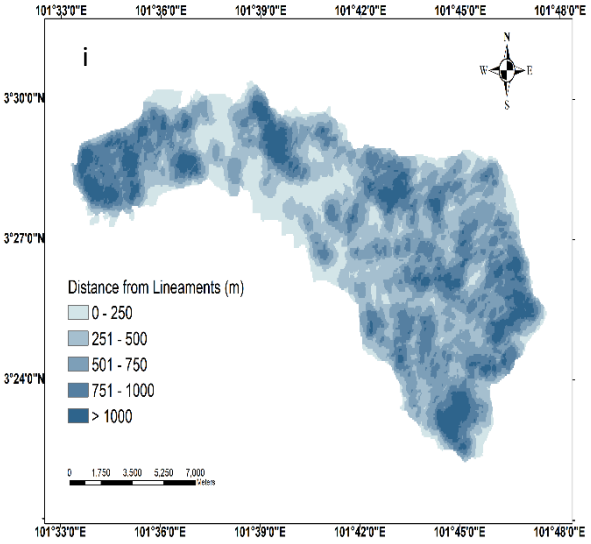
regulating the concentration and diffusion of surface and groundwater in slopes **(Zhao et al., 2022)**. The curvature map was created from the digital elevation model of the area and divided into five groups (1) very concave (< −5), (2) concave (−5 to −1), (3) flat (−1 to 1), (4) convex (1 to 5), and (5) very convex (> 5) as shown in **Fig. 3c**. According to the distribution of landslides across the curvature classes, roughly 52.18% of landslides occurred in flat zones, 23.91% in concave zones, and 23.91% in convex zones. This implies that the majority of landslides typically happen on surfaces that are transitional or fairly level, where drainage is poor, and slope instability is likely to arise **(Table 4).**

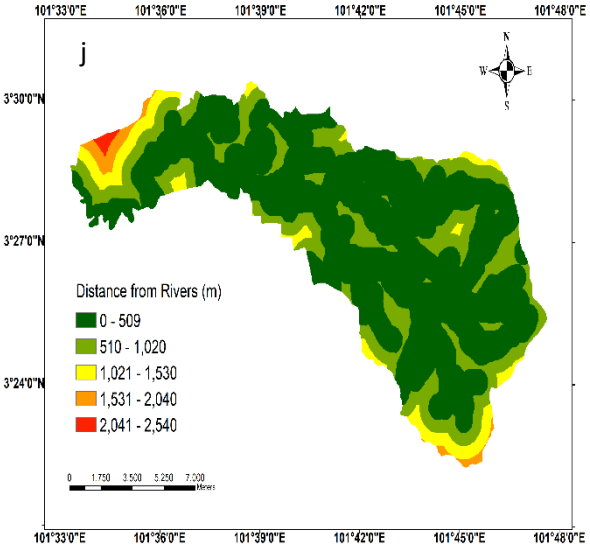
3.2.4 Elevation (DEM)

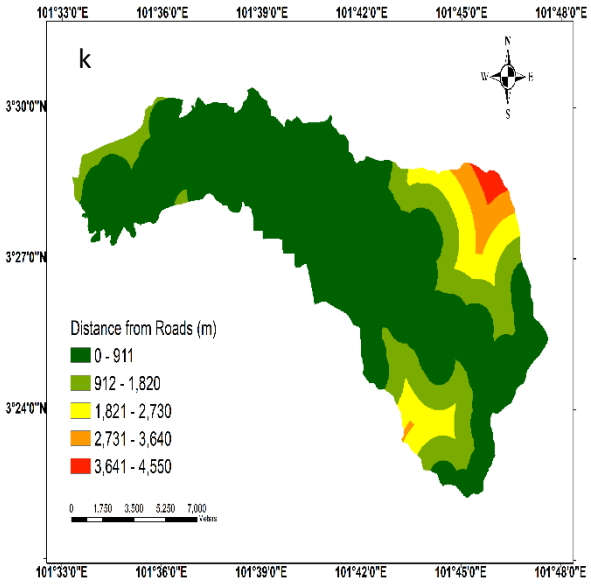
The research area's DEM from mean sea level (MSL) is shown in **Fig. 3d**. Elevation has a major effect on the earth's surface and topographic features. These characteristics usually explain the spatial variation of some processes that occur within the landscape, such as vegetation patterns driven by topography. The influence of elevation on landslides is often treated indirectly or compared to other factors with direct causative relationships associated with the occurrence of Landslides **(Pei et al., 2023)**. Elevation is part of the factors contributing to instability on each slope as one of the layers. It indirectly affects many landslide factors, including temperature, freeze–thaw cycles, thawing, annual rainfall, and high rainfall. It is essential to emphasize that it will typically predominate on steep sites such as valley walls, river gorges, mountain slopes, and the toe of cliffs. Hence, understanding terrain & terrain-derived factors is requisite for landslide hazard mapping. In this regard, the Shuttle Radar Topography Mission (SRTM) derived Digital Elevation Model (DEM) of 30 m resolution available from the USGS Earth Explorer website was used to create various factor layers. In terms of altitude, the land's maximum elevation is 1870 m and the minimum elevation is 7m; so, there is a total difference in altitude of 1863m. An elevation map was obtained in this study from a digital elevation model (DEM) and classified into the following five classes: (1) 7–256, (2) 257–592, (3) 593–899, (4) 900–1,270, and (5) 1,280–1,870 m. An assessment of the landslides' geographical distribution revealed that as many as 80.43% of the overall landslides took place at a high altitude (1,280–1,870 m), while 15.22% and 4.35% occurred within the 593–899 m and 900–1,270 m elevation classes, respectively. This indicates that landslides occur more frequently in the higher-elevation areas of Batang Kali, where steep slopes and ample rainfall may aggravate slope instability **(Table 4)**.

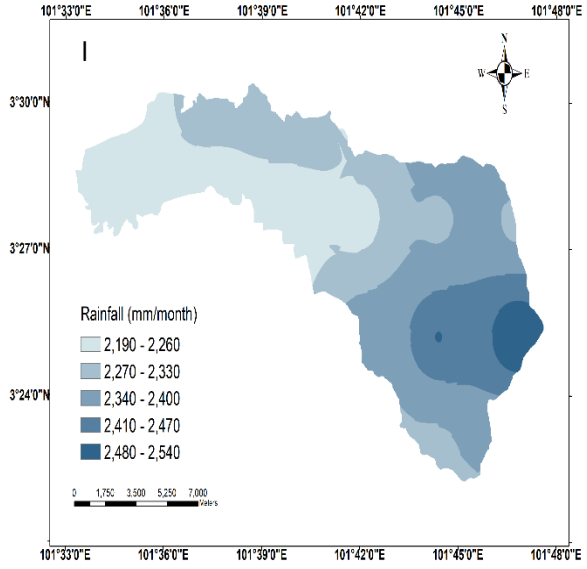


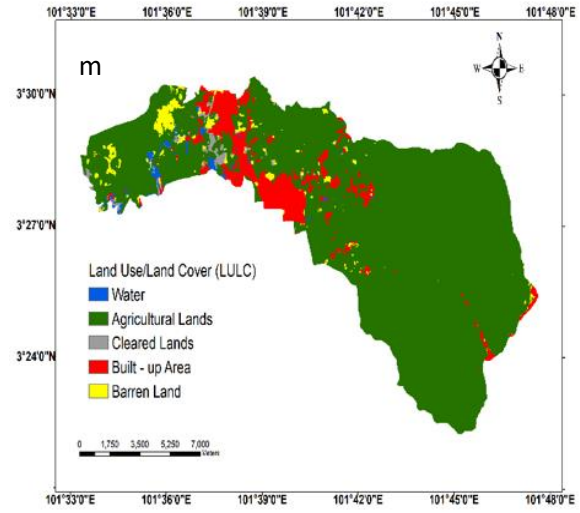

c
Curvature (m⁻ ¹)
< -5
-5 - -1
-1 - 1
1 - 5
> 5
d
Elevation (m)
7 - 256
257 - 592
593 - 899
900 - 1,270
1,280 - 1,870
e
TWI
0.693 - 4.88
4.89 - 6.89
6.9 - 9.74
9.75 - 13.6
13.7 - 22.1
f
TRI
0.111 - 0.383
0.384 - 0.462
0.463 - 0.532
0.533 - 0.611
0.612 - 0.889
g
STI
0 - 163
164 - 749
750 - 1,790
1,800 - 2,920
2,930 - 4,150
h
SPI
-6.91 - -2.45
-2.44 - -0.662
-0.661 - 0.995
0.996 - 3.54
3.55 - 9.34

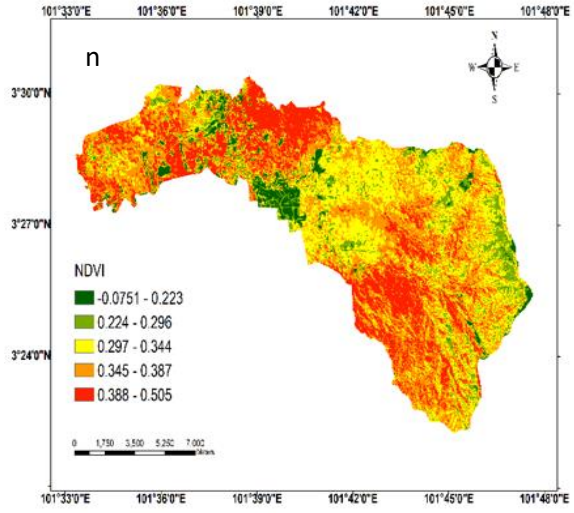

i
Distance from Lineaments (m)
0 - 250
251 - 500
501 - 750
751 - 1000
> 1000


j
Distance from Rivers (m)
0 - 509
510 - 1,020
1,021 - 1,530
1,531 - 2,040
2,041 - 2,540


k
Distance from Roads (m)
0 - 911
912 - 1,820
1,821 - 2,730
2,731 - 3,640
3,641 - 4,550


l
Rainfall (mm/month)
2,190 - 2,260
2,270 - 2,330
2,340 - 2,400
2,410 - 2,470
2,480 - 2,540


m
Land Use/Land Cover (LULC)
Water
Agricultural Lands
Cleared Lands
Built - up Area
Barren Land


n
NDVI
-0.0751 - 0.223
0.224 - 0.296
0.297 - 0.344
0.345 - 0.387
0.388 - 0.505

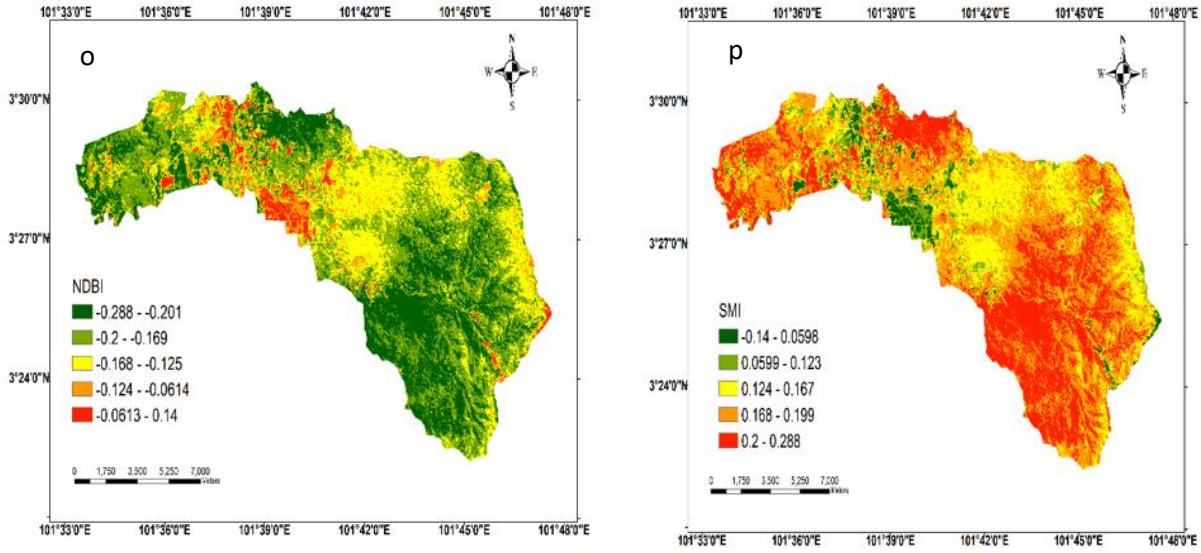


Figure 3. Landslide influencing factors used in this study area: (a) Slope (°), (b) Aspect (°), (c) Curvaturem^{-1}), (d)Elevation (m), (e) TWI, (f) TRI, (g) STI, (h) SPI, (i) Distance from Lineaments (m), (j) Distance from Rivers (m), (k) Distance from Roads (m), (l) Rainfall (mm/month), and (m) LULC, (n) NDVI, (o) NDBI, (p) SMI

3.2.5 Topographic Wetness Index (TWI)

The TWI is a single theoretical element that could be used to describe the pattern of moisture within one or more catchments, as it represents an index of flow accumulation at each point across a regional landscape **(Öztürk, 2025)**. According to **(Punyal and Kumar, 2026)**, it is reported that TWI is a ratio of the areas draining to a point in the landscape to slope steepness **(Kumar et al., 2025)**. TWI values are used to estimate soil moisture, which deals with the saturation condition of surface and subsurface forms on land slopes concerning slope instability. High values of this index are mainly used in landslide masses and, normally, are used for the topographic control of hydrological processes. The TWI is computed using Eq. (1):

$$\text{TWI} = \text{Ln}\left(\frac{a}{tan\beta}\right) \quad (1)$$

Where a represents the local upslope contributing area per unit contour length, and β represents the slope angle at a given point. The upslope contributing area (a) was obtained from flow accumulation analysis after filling depressions, and the flow direction was estimated using the digital elevation model (DEM) in this study. The angle of slope (β) was first estimated in degrees from the DEM and then transformed into radians to produce the tangent of the angle of inclination. The resulting upslope contributing area and tangent of the slope angle were subsequently used to calculate the TWI. Five distinct TWI classes, with values ranging from 0.693 to 22.1, were created from the research region **(Fig. 3e)**. The classes are: (1) 0.693 - 4.88, (2) 4.89 - 6.89, (3) 6.9 - 9.74, (4) 9.75 - 13.6, and (5) 13.7 - 22.1 as shown in **Fig. 3e**. Approximately 47.83% of the identified landslide locations were associated with the 0.693–4.88 and 4.89–6.89 TWI classes, respectively, while 4.34% occurred within the 6.9–9.74 class **(Table 4)**.

3.2.6 Topographic Ruggedness Index (TRI)

The TRI, which is the difference between the height of one pixel and the eight pixels surrounding it, was introduced by **(Ersayin, 2025)**. The TRI is computed using Eq. (2).

$$TRI = (Smooth - Min) / (Max - Min) \quad (2)$$

Where Smooth is the focal mean elevation, Min is the focal minimum elevation, and Max is the focal maximum elevation within the range. These parameters were calculated using focal statistics on a DEM with the same neighborhood, creating raster images of maximum, minimum, and mean elevation. The mean elevation was used as the smoothed elevation (Smooth). The TRI was then calculated using the Raster Calculator according to Eq. (2). The TRI map was constructed from 5 classes: (1) 0.111 - 0.383, (2) 0.384 - 0.462, (3) 0.463 - 0.532, (4) 0.533 - 0.611, and (5) 0.612 - 0.889 as shown in **Fig. 3f**. Approximately 47.83% of the landslide area occurred within the 0.463–0.532 TRI class, followed by 23.91% within the 0.384–0.462 class and 19.56% within the 0.533–0.611 class. The lowest proportions, 4.35% each, were recorded within the 0.111–0.383 and 0.612–0.889 classes. These findings suggest that somewhat difficult terrain, where moderate slopes interact with partial soil wetness to produce weak stability, is where landslides are most common **(Table 4).**

3.2.7 Sediment Transport Index (STI)

Sediment transport index (STI) is one of the ways to quantify sediment mobility. Data on the transport capacity, accumulation, and spatial distribution of sediments are provided by the STI **(Das et al., 2026).** In regions with heavy runoff, more sediment is carried than in regions with low runoff. The STI is computed using Eq. (3), where

$$\text{STI} = \left(\frac{AS}{22.13}\right)^{0.6} \left(\frac{Sin\ \beta}{0.0896}\right)^{1.3} \quad (3)$$

Here, "As" stands for the flow accumulation, and "b" refers to the slope. STI outputs are classified into five classes: (1) 0 - 163, (2) 164 - 749, (3) 750 - 1,790, (4) 1,800 - 2,920, and (5) 2,930 - 4,150 as shown in **Fig. 3g**. An examination of the distribution of landslides in relation to the Sediment Transport Index (STI) revealed that 43.48% of landslides happened in regions with low or no STI, while roughly 56.52% of landslides happened in places with high STI values—areas with high eroding capacity and vigorous water flow. According to these findings, greater erosion and a weakened slope base are two major ways in which high runoff energy contributes to slope destabilization **(Table 4)**.

3.2.8 Stream Power Index (SPI)

Based on the assumption that the discharge (q) is directly proportional to the catchment area (As), the Stream Power Index (SPI) is a tool for calculating the erosive potential of surface water. Two factors control the SPI value: the slope of the land and the viscosity of the terrain slope. The erosive force of slope surface runoff is reflected in the SPI, a metric generated from digital elevation models (DEMs) that may affect the occurrence of landslides **(Lai and Qi, 2026**; **Zighmi et al., 2025).** The SPI is computed using Eq. (4).

$$\text{SPI} = As * tan\ \beta \quad (4)$$

The SPI layer was extracted into five classes: (1) -6.91 - -2.45, (2) -2.44 - -0.662, (3) -0.661 - 0.995, (4) 0.996 - 3.54, (5) 3.55 - 9.34 as shown in **Fig. 3h**. According to a study comparing the distribution of landslides to the Stream Power Index (SPI), approximately 43.47% of landslides occurred in regions with medium SPI values, 32.61% in regions with high SPI values, 19.57% in regions with low SPI values, and 4.35% in regions with very low SPI values. According to these findings, landslides are more frequent in regions with moderate to high runoff, where soil cohesiveness deteriorates and base slope erosion rises **(Table 4)**.

3.2.9 Distance from Lineaments

The research area's structural information or structural geology is one of the elements affecting the assessment of landslide susceptibility. It is commonly known that one of the main elements influencing the incidence of landslides is the area's structural geology **(Tukku et al., 2025)**. Joints, faults, foliations, bedding planes, and lines of weakness that predate the rock body are examples of structural discontinuities. These weak lines, which are frequently seen in broken areas, are probably places where vegetation grows and rainwater collects. Not only do they serve as guidelines, but they also have a substantial impact on terrain permeability and, in turn, slope stability, as well as the structures of surface materials **(Panchal and Srivastava, 2026)**. Distance from lineament mapping can be used as one approach to including structural elements in the assessment of susceptibility to landslides. A continuous distance surface was constructed by calculating the minimum straight-line (Euclidean) distance of each raster cell to the nearest line. The distance in meters from the lines was computed with the Euclidean distance tool in ArcGIS. Extract distance from lineaments map of the faults to 5 classes: (1) 0–250, (2) 251–500, (3) 501–750, (4) 751–1,000, and (5) >1,000 m, as shown in **Fig. 3i**. About 28.26% of landslides occurred within 501–750 meters of lineaments, followed by 23.91% in the 251–500m and 751–1,000 m classes, according to an analysis of the link between landslide distribution and distance from lineaments. The percentage was 8.70% in places more than 1,000 m from lineaments and 15.22% in areas within 0–250 m of lineaments. According to these findings, the majority of landslides happen in locations that are halfway between lineaments, where the impact of structural weakness is still noticeable as long as the slope is active **(Table 4)**.

3.2.10 Distance from Rivers

The distance to the river is another element that has a direct impact on the likelihood of landslides **(Ružek and Šilhán, 2024)**. Since water runoff actively contributes to land mass movements, it is one of the elements that raises the risk of slope instability **(Liu et al., 2025).** The Euclidean Distance tool in ArcGIS was applied to determine the distance to the river in meters per pixel between the research area and the closest watercourse line. The distance map from the river was generated with five classes: (1) 0 - 509, (2) 510 - 1,020, (3) 1,021 - 1,530, (4) 1,531 - 2,040, and (5) 2,041 - 2,540 m as shown in **Fig. 3j**. An examination of the distribution of landslides by distance from rivers revealed that almost 39.13% of them happened between 0 and 509 meters from rivers, with the 510–1,020 m and 1,021–1,530 m categories following closely behind, each with 28.26% of the total. The regions that were furthest from rivers (2,041–2,540 m) had the lowest percentage (4.35%). According to these findings, the majority of landslides occur close to waterways, where slope stability is weakened by soil saturation and river erosion **(Table 4).**

3.2.11 Distance from Roads

Slope stability may be influenced by the distance from roads **(Wood and Jones, 2025)**. Slope instability is also caused by filled and excavated slopes, as well as by inadequate road drainage systems connected to road construction **(Kucuker, 2025)**. Slopes that would otherwise be stable may collapse as a result of road construction activities, such as soil excavation, the application of additional loads, and plant removal. In this study, the Euclidean Distance tool in ArcGIS was used to calculate the distance from the road, or the distance between each pixel in the study region and the nearest road. Roads Distance from roads was classified into five categories: (1) 0 - 911, (2) 912 - 1,820, (3) 1,821 - 2,730, (4) 2,731 - 3,640, and (5) 3,641 - 4,550 m as shown in **Fig. 3k**. Approximately 43.48% of landslides occurred within a distance of 0–911 m from roads, followed by the 912–1,820 m category at 28.26%. The percentage did not surpass 15.22% in areas farther than 2.7 km from roads, according to an analysis of the relationship between landslide distribution and distance from roads. These findings suggest that human activities like slope cutting, water accumulation, and traffic vibrations degrade soil stability, which is why landslides are concentrated next to roadways **(Table 4)**.

3.2.12 Rainfall

The onset of landslides is significantly influenced by the amount and duration of rainfall **(Ghosh and Saha, 2025)**. The rainfall map of the area was created using the Inverse Distance Weighting (IDW) technique. A rainfall map was prepared consisting of five classes: (1) 2,190 - 2,260, (2) 2,270 - 2,330, (3) 2,340 - 2,400, (4) 2,410 - 2,470, and (5) 2,480 - 2,540 as shown in **Fig. 3l**. Around 47.82% of landslides occurred in areas with an annual rainfall of 2,340–2,400 mm, followed by areas with high rainfall (2,410–2,470 mm) at 19.57%, according to an examination of the distribution of landslides in relation to rainfall intensity. According to these findings, landslides are more prevalent in areas with moderate to high rainfall because ongoing precipitation raises soil moisture and weakens soil cohesiveness, both of which enhance the risk of landslides **(Table 4)**.

3.2.13 Land Use/Land Cover (LULC)

Land use alters the characteristics of the soil and modifies its behavior; it plays a significant role in slope instability **(Pramanik and Hegde, 2026)**. For the study of landslide susceptibility, a land use layer was one of the factors that contributed, and it was developed and extracted from the 2022 Esri Land Cover dataset, which was derived from Sentinel-2 satellite imagery at 10 m spatial resolution. The reason for selecting the 2022 dataset is that it is a reflection of the land cover circumstances for the same year as the catastrophic landslide event happened in Batang Kali on 16 December 2022, therefore giving a time-appropriate representation of the land use/land cover conditions for the study. The classification of the land cover map in the research region was based on the classification methodology used by the Department of Survey and Mapping Malaysia (JUPEM), where five main land cover types were identified: Agricultural Lands, Cleared Lands, Built-up Area, Barren Land, and Water, as shown in **Fig. 3m**. Approximately 91.30% of landslides happened on agricultural lands, whereas just 8.70% happened in built-up areas, according to a landslide distribution analysis by LULC. These findings suggest that human activities like

plowing, vegetation removal, and irrigation water seepage, which raise soil saturation and reduce soil cohesiveness, make agricultural fields more vulnerable to landslides **(Table 4)**.

3.2.14 Normalized Difference Vegetation Index (NDVI)

The NDVI effectively monitors growth and vegetation levels within a specific area **(Wang et al., 2026; Lusiana et al., 2026)**. The NDVI is derived from the reflectance measurements of the red band (Band 4; 0.64–0.67 μm) and the near-infrared (NIR) band (Band 5; 0.85–0.88 μm) of Landsat 8. The NDVI is computed using Eq. (5).

$$NDVI = (NIR - RED)/(NIR + RED) \quad (5)$$

The values of this indicator range from −1 to +1. The map of the NDVI was created with five classes: (1) −0.0751–0.223, (2) 0.224–0.296, (3) 0.297–0.344, (4) 0.345–0.387, and (5) 0.388–0.505, as shown in **Fig. 3n**. Approximately 43.48% of the landslides occurred in areas with medium to high vegetation cover (NDVI = 0.345–0.387), followed by areas with medium vegetation cover (19.56%; NDVI = 0.297–0.344). In contrast, 13.04% of the landslides occurred in areas with high vegetation cover (NDVI = 0.388–0.505). These findings indicate that landslides were more frequently distributed in areas with medium to high vegetation cover, possibly due to vegetation cover loss following previous landslides or human activities on the slopes **(Table 4)**.

3.2.15 Normalized Difference Built-Up Index (NDBI)

Built-up or impermeable regions can be identified and categorized using the NDBI index **(Ramdani et al., 2025)**. Built-up areas are shown by positive NDBI values, plant cover is indicated by values around zero **(Liu et al., 2023)**, and water bodies are represented by negative values. The NDBI is computed using Eq. (6).

$$NDBI = (MIR - NIR)/(MIR + NIR) \quad (6)$$

Where MIR is the wavelength of band 6 of Landsat 8, equal to 1.57-1.65 μm, and NIR is band 5 (of Landsat 8 OLI, wavelength 0.85-0.88 μm) **(Badapalli et al., 2025).**
The NDBI map was produced in five classes: (1) -0.288 - -0.201, (2) -0.2 - -0.169, (3) -0.168 - -0.125, (4) -0.124 - -0.0614 and (5) -0.0613 - 0.14 as shown in **Fig. 3o**. According to an NDBI analysis, areas with dense vegetation cover and low NDBI values (-0.288 to -0.201) accounted for about 39.13% of landslides. In contrast, just 8.70% of landslides happened in populated metropolitan areas, whereas 28.26% happened in places that were in between exposed and vegetated areas. These findings suggest that landslides are less common in stable, level urban areas and more often in naturally occurring places with vegetation and slopes **(Table 4)**.

3.2.16 Soil Moisture Index (SMI)

The distribution of rainfall has tremendous influence on soil moisture **(Bayable et al., 2025; Machireddy, 2025)**. Two important factors affecting the soil moisture index are the vegetation cover index and the surface temperature of the ground in the research area. Landsat 8 images with 30 m spatial resolution available from the USGS Earth Explorer website were used to construct the NDVI using the red and near-infrared (NIR) spectral

bands, and the land surface temperature (LST) was retrieved from the thermal infrared (TIR) band. The SMI was determined by applying Eq. (7) **(Adamala et al., 2025)**. The SMI index was generated on a pixel-to-pixel basis from LST raster data derived from Landsat 8 satellite images. Maximum LST value (LSTmax) and minimum LST value (LSTmin) were extracted from the raster LST data in the study area. These values were applied in Equation (7) to normalize the LST values and produce the SMI raster data. The resulting SMI raster data was then analyzed in ArcGIS and later classified into five classes by utilizing a manual classification approach.

$$SMI = \frac{LST_{max} - LST}{LST_{max} - LST_{min}} \quad (7)$$

Where LST is the land surface temperature of each pixel and $LST_{max} and\ LST_{min}$ are the maximum and minimum LST values in the study area. The SMI map was constructed using the ArcGIS program. Then we used a manual classification method to divide the map into five classes as shown in **Fig. 3p.** The analysis of the distribution of landslides based on the Soil Moisture Index (SMI) shows that 43.47% of landslides occurred in areas with high SMI values (0.2-0.288), then 28.26% in areas with values ranging from 0.124 to 0.167, and then 19.57% in areas with values ranging from 0.168 to 0.199. The lowest percentage of landslides, 8.70%, was recorded in the locations with values between -0.14 and 0.0598, while no landslides were recorded in the values category between 0.0599 and 0.123 **(Table 4)**.

4. ANALYSIS OF LANDSLIDE SUSCEPTIBILITY

The landslide susceptibility analyses in this work were conducted by employing the AHP model. The factors causing landslides in the Batang Kali area were determined before the analysis. Satellite images and a landslide inventory map were used to identify landslide regions.

4.1 Analytical Hierarchy Process (AHP)

The Analytic Hierarchy Process (AHP) is a multi-criteria decision-making technique based on quantitative and qualitative factors **(Saaty, 2003; Abubakar et al., 2025).** An unstructured, complex problem is broken down into simple components using AHP. These components are then arranged hierarchically and given a numerical value that represents their relative importance, before the priorities assigned to each transaction are determined **(Gacu et al., 2025)**. Regional planning **(Kara and Iranmanesh, 2025)**, landslide susceptibility study **(Mao et al., 2025)**, site selection **(Sisay et al., 2025)**, and suitability analysis **(Al-Awadhi et al., 2025)** have all made extensive use of the analysis of hazards and threats approach **(Lai and Qi, 2026)**. Several studies have effectively mapped landslide susceptibility using this method **(Bensalem et al., 2026**; **Gebrehiwot et al., 2025**; **Ali et al., 2025).**

Analytic Hierarchy Process (AHP) entails creating a hierarchy of decision factors by breaking the problem down into primary and secondary objectives. Then, pairwise comparisons are performed and compared in a matrix to ascertain the consistency ratio and the weight of each factor **(Ait Omar et al., 2025)**. A pairwise comparison matrix is generated for every factor at every level once the hierarchy has been established. This allows each factor's significance in relation to all other factors **(Khan et al., 2026)**. If there is a direct relationship

between the factors, then each factor in AHP is rated against all other factors by being assigned a score between 1 and 9. On the other hand, the reciprocals 1/2 and 1/9 have different values **(Saaty, 1977)**. Based on historical landslide data as well as an extensive assessment of past studies on landslide susceptibility in the study area, a preliminary 16 × 16 pairwise comparison matrix was constructed. The initial matrix was then assessed by experts from Malaysian Government agencies and technical institutes who have experience in the fields of geology, geotechnical engineering, surveying, soil resources, and geospatial information. The experts evaluated the relative importance of the sixteen landslide-influencing factors using Saaty's fundamental 1–9 scale and recommended adjustments to some of the pairwise judgments based on their practical expertise. The proposed alterations were integrated into the initial matrix to obtain the final pairwise comparison matrix for AHP analysis **(Table 1)**.

Standardizing the elements, figuring out each factor's weight, and gathering the criteria are the three crucial processes in the AHP process. In the first step, to make comparisons easier, the factors and their spatial visualization must be connected to a similar scale. If the factor class has no influence, the susceptibility level is set to 0. The second stage was to build a comparison matrix, comparing each component to the others based on their importance. The quality of the comparison is characterized by the Consistency Ratio (CR), which is obtained by dividing the Consistency Index (CI) by the Random Index (RI) **(Aguarón and Moreno-Jiménez, 2003) (Table 2)**, as stated in the following Eq. (8).

$$CR = CI / RI \quad (8)$$

Table 1. Pairwise comparison matrix for the AHP analysis

Factors	Rainfall	Slope	Aspect	SPI	SMI	TWI	TRI	Distance from Roads	Curvature	STI	LULC	NDVI	Elevation	Distance from Lineaments	Distance from Rivers	NDBI
Rainfall	1	2	3	3	2	3	3	3	3	3	4	4	7	9	9	9
Slope	1/2	1	1	1	1	1	1	1	1	2	2	2	3	5	6	9
Aspect	1/3	1	1	1	1	1	1	1	1	1	2	2	3	5	5	8
SPI	1/3	1	1	1	1	1	1	1	1	1	2	2	3	5	5	8
SMI	1/2	1	1	1	1	1	1	1	1	1	2	2	3	5	5	8
TWI	1/3	1	1	1	1	1	1	1	1	1	2	2	3	4	5	8
TRI	1/3	1	1	1	1	1	1	1	1	1	2	2	3	4	5	8
Distance from Roads	1/3	1	1	1	1	1	1	1	1	1	2	2	3	4	5	7
Curvature	1/3	1	1	1	1	1	1	1	1	1	1	1	2	4	4	7
STI	1/3	1/2	1	1	1	1	1	1	1	1	1	1	2	4	4	6
LULC	1/4	1/2	1/2	1/2	1/2	1/2	1/2	1/2	1	1	1	1	2	3	3	5
NDVI	1/4	1/2	1/2	1/2	1/2	1/2	1/2	1/2	1	1	1	1	2	3	3	5
Elevation	1/7	1/3	1/3	1/3	1/3	1/3	1/3	1/3	1/2	1/2	1/2	1/2	1	2	2	3
Distance from Lineaments	1/9	1/5	1/5	1/5	1/5	1/4	1/4	1/4	1/4	1/4	1/3	1/3	1/2	1	1	2
Distance from Rivers	1/9	1/6	1/5	1/5	1/5	1/5	1/5	1/5	1/4	1/4	1/3	1/3	1/2	1	1	2
NDBI	1/9	1/9	1/8	1/8	1/8	1/8	1/8	1/7	1/7	1/6	1/5	1/5	1/3	1/2	1/2	1

Table 2. Random Index (RI) values used for AHP consistency assessment

N	1	2	3	4	5	6	7	8	9	10	11	12	13	14	15	16
RI Value	0.000	0.000	0.525	0.882	1.115	1.252	1.341	1.404	1.452	1.49	1.484	1.535	1.555	1.570	1.583	1.595

A consistency ratio of less than 0.10 indicates a matrix with acceptable consistency. A low consistency ratio (less than 0.10) means that each factor's weight is appropriate. Step 3 involves extracting a landslide susceptibility map using a weighted linear combination (WLC). This map can be utilized in GIS and is among the most popular decision rules. The sixteen factor layers are multiplied by their respective weight values and added together in WLC.

5. RESULTS AND DISCUSSION

Using the GIS-AHP model, a landslide susceptibility map was made in the research area and divided into five classes: very low, low, moderate, high, and very high. The distribution of landslide susceptibility classes in terms of area and percentage in the study region was developed based on the application of the AHP model approach.

The spatial association between landslides and influencing factors is shown in **Table 4,** Relative weights of the causal factors are determined from the pairwise comparison matrix in the AHP model. These results indicate that rainfall is the most important factor with a value of 0.1801, followed by Slope, SMI, and Aspect with values of 0.0828, 0.0773, and 0.0753, respectively. In soil or other cohesionless strata, the shear strength often decreases with an increase in slope. SPI, TWI, TRI, and Distance from Roads showed that the AHP values were 0.0753, 0.0743, 0.0743, and 0.0736, respectively. In the case of Curvature and STI, they have 0.0657 and 0.0625 AHP values , respectively. The curvature region will thus elevate the moisture content, which will remain saturated, thereby exacerbating erosion and diminishing slope stability. Also, LULC, NDVI, and Elevation analyses showed that the AHP values were 0.0451, 0.0450, and 0.0268, respectively. The AHP index for Distance from Lineaments is 0.0164, while Distance from Rivers shows 0.0156, and NDBI shows 0.0099 (which are less important) **(Table 4)**. The most important factor is rainfall, which is consistent with Malaysia's tropical climate. Prolonged heavy rainfall raises pore water pressure, decreases soil shear resistance, and results in slope collapses. Similarly, increased soil moisture contributes to decreased stability of the slope materials, while the angle of inclination plays a critical role in regulating the gravitational forces acting on them. These findings are in line with earlier research on landslide susceptibility carried out in tropical and mountainous regions, which found that rainfall, slope, and soil moisture were important determinants of landslide incidence. This study reports a consistency ratio (CR) of 0.0076, which is less than 0.10, demonstrating an exceptional level of consistency for the matrix, adequate for ascertaining the weight of each factor. Upon completion of the analysis, the frequency of class distributions for each layer was ascertained, and a landslide susceptibility map (LSM) was generated utilizing the AHP model, as shown in **Fig. 4**.

The landslide susceptibility map produced by the AHP approach is displayed on **Fig. 4**. Using the natural break classification method, it was classified into five relative susceptibility zones: very low, low, medium, high, and very high. The east of the research region has a very high risk of landslides, as shown in **Fig. 4.**

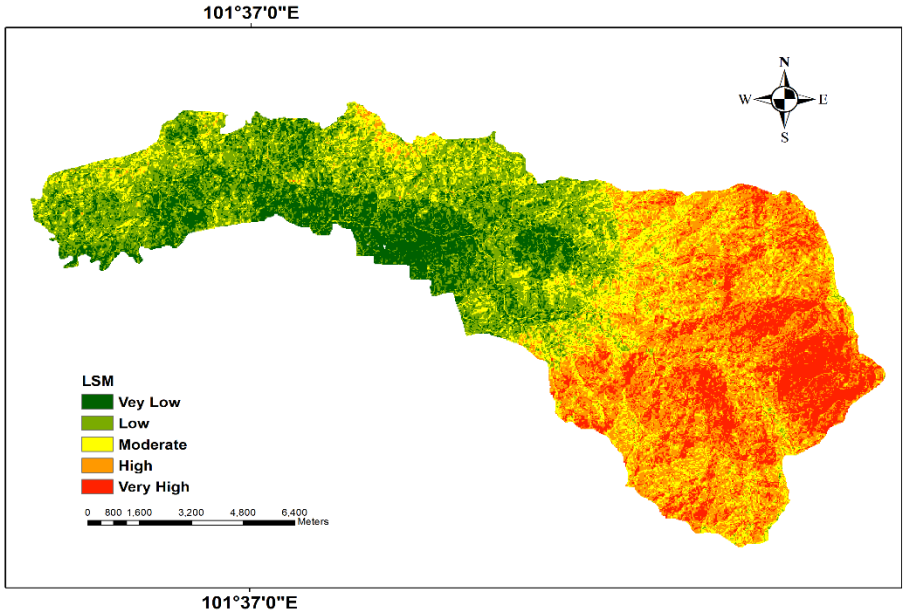


Figure 4. Landslide susceptibility map generated from the AHP model

Most of this area is made up of agricultural land. The research area's extreme north, as well as its southeastern and northern regions, were shown to have many moderately landslide-prone places. The center and southwest of the research region are primarily areas with low landslide susceptibility. **Table 3** shows that landslide susceptibility was very low in 23.26 km^2 of the overall region. 40.94 km^2 of the total area was found to be of low landslide susceptibility. The moderately susceptible zone represents 32.01 km^2 of the total area. Of the entire research region, 39.45 km^2 is classified as high susceptibility areas, and 22.78 km^2 as very high susceptibility areas.

Table 3. The different susceptibility zones of the study area (AHP method)

Method	Susceptibility zones	Area (km^2)	Landslide distribution (%)
AHP	Very Low	23.26	14.68
	Low	40.94	25.84
	Moderate	32.01	20.20
	High	39.45	24.90
	Very High	22.78	14.38

Table 4. Relative weights and class distribution of the landslide influencing factors derived from the AHP model

	Factor	Class	km^2 of total area	% of Landslide area	Final Weights
1	Slope	0–10°	46.81	4.35	0.0828
		10–20°	46.18	8.70	
		20–30°	38.51	43.47	
		30–40°	22.85	43.48	
		>40°	4.09	0.00	
2	Rainfall	2,190 - 2,260	37.06	4.35	0.1801
		2,270 - 2,330	38.02	13.04	
		2,340 - 2,400	50.16	47.82	

		2,410 - 2,470	23.2	19.57	
		2,480 - 2,540	10	15.22	
3	Aspect	Flat (-1)	13.18	0.00	0.0753
		North (0-22.5)	12.13	4.35	
		Northeast (22.5-67.5)	10.67	4.35	
		East (67.5-112.5)	11.50	0.00	
		Southeast (112.5-157.5)	13.91	0.00	
		South (157.5-202.5)	16.38	0.00	
		Southwest (202.5-247.5)	19.70	4.35	
		West (247.5-292.5)	21.92	28.26	
		Northwest (292.5-337.5)	20.70	32.61	
		North (337.5-360)	18.35	26.08	
4	Stream Power Index (SPI)	-6.91 - -2.45	17.08	4.35	0.0753
		-2.44 - -0.662	56.22	19.57	
		-0.661 - 0.995	55.24	43.47	
		0.996 - 3.54	24.30	32.61	
		3.55 - 9.34	5.60	0.00	
5	Soil Moisture Index (SMI)	-0.14 - 0.0598	4.75	8.70	0.0773
		0.0599 - 0.123	9.80	0.00	
		0.124 - 0.167	36.45	28.26	
		0.168 - 0.199	60.34	19.57	
		0.2 - 0.288	47.10	43.47	
6	Topographic Wetness Index (TWI)	0.693 - 4.88	67.00	47.83	0.0743
		4.89 - 6.89	58.92	47.83	
		6.9 - 9.74	19.64	4.34	
		9.75 - 13.6	10.45	0.00	
		13.7 - 22.1	2.43	0.00	
7	Topographic Ruggedness Index (TRI)	0.111 - 0.383	16.2	4.35	0.0743
		0.384 - 0.462	38.79	23.91	
		0.463 - 0.532	51.19	47.83	
		0.533 - 0.611	38.33	19.56	
		0.612 - 0.889	13.93	4.35	
8	Distance from Roads	0 - 911	86.58	43.48	0.0736
		912 - 1,820	31.56	28.26	
		1,821–2,730	21.72	15.22	
		2,731–3,640	13.00	13.04	
		3,641–4,550	5.58	0.00	
9	Curvature	< -5	1.43	0.00	0.0657
		-5 - -1	27.54	23.91	
		-1 - 1	104.05	52.18	
		1 - 5	25.29	23.91	
		> 5	0.13	0.00	
10	Sediment Transport Index (STI)	0 - 163	93.50	43.48	0.0625
		164 - 749	16.85	0.00	
		750 - 1,790	16.11	0.00	
		1,800 - 2,920	16.01	0.00	
		2,930 - 4,150	15.97	56.52	
11	Land Use/Land Cover (LULC)	Water	1.32	0.00	0.0451
		Agricultural Lands	137.95	91.30	
		Cleared Lands	1.71	0.00	

		Built-up Area	13.48	8.70	
		Barren Land	3.98	0.00	
12	Normalized Difference Vegetation Index (NDVI)	-0.0751 - 0.223	6.21	8.70	0.0450
		0.224 - 0.296	15.94	15.22	
		0.297 - 0.344	45.32	19.56	
		0.345 - 0.387	53.03	43.48	
		0.388 - 0.505	37.94	13.04	
13	Elevation	7 - 256	8.87	0.00	0.0268
		257 - 592	20.97	0.00	
		593- 899	44.83	15.22	
		900- 1,270	50.73	4.35	
		1,280- 1,870	33.04	80.43	
14	Distance from Lineaments	0–250	22.22	15.22	0.0164
		251–500	42.81	23.91	
		501–750	44.64	28.26	
		751–1000	34.14	23.91	
		>1000	14.63	8.70	
15	Distance from Rivers	0 - 509	62.16	39.13	0.0156
		510 - 1,020	46.77	28.26	
		1,021 - 1,530	30.38	28.26	
		1,531 - 2,040	13.91	0.00	
		2,041 - 2,540	5.22	4.35	
16	Normalized Difference Built-up Index (NDBI)	-0.288 - -0.201	44.46	39.13	0.0099
		-0.2 - -0.169	60.27	23.91	
		-0.168 - -0.125	38.66	28.26	
		-0.124 - -0.0614	10.13	0.00	
		-0.0613 - 0.14	4.92	8.70	

6. VALIDATION OF PREDICTIVE MODELS

The Receiver Operating Characteristics (ROC) curve is a useful tool for evaluating the accuracy of forecasting systems and probabilistic and deterministic results **(Riesthuis and Otgaar, 2025)**. The ROC curve test was employed as a validation technique in this study. The ROC curve test was employed as a validation technique in this study. The GIS-AHP-based landslide susceptibility map was validated using the available inventory of 46 identified landslide locations as reference samples for the ROC–AUC analysis. The ROC curve was constructed, and the AUC was determined using ArcGIS software with the ArcSDM extension. The model's ability to discriminate between landslide-prone and non-landslide-prone areas is indicated by the area under the curve (AUC) **(Abdulahi et al., 2026)**. The false positive rate is displayed on the x-axis, and the true positive rate on the y-axis. This is termed a ROC curve, and a larger area under the curve indicates better prediction performance. The value varied from 0.5, signifying a random prediction illustrated by the diagonal line, to 1, denoting an exceptional prediction that can aggregate the relative ranks of each prediction type **(Lee et al., 2025)**. This study demonstrated that the model accurately predicted the proportion of unstable pixels, as well as the effectiveness of validation regarding the anticipated unstable pixels. The area beneath the curve can qualitatively evaluate the precision of the forecast **(Martin et al., 2025)**. The area under the curve (AUC) of the landslide susceptibility map generated using the AHP model was 0.722, indicating a prediction accuracy of 72.2%, as assessed using the ROC. The ROC-AUC value of 72.2% suggests that the AHP model has an

appropriate level of prediction power for the separation of landslide-prone and non-landslide-prone regions. While the model does not provide outstanding prediction performance, the result shows the effectiveness of incorporating numerous influencing factors in an AHP-based GIS framework for assessing landslide susceptibility at the regional level. The ROC curve analysis indicates that the AHP model employed in this study exhibits a good level of prediction accuracy, thereby validating its utility in assessing the relative ranking of landslide-prone regions and enhancing the credibility of the resultant susceptibility map.

7. CONCLUSIONS

Mapping landslide susceptibility is crucial for reducing disaster risks and supporting sustainable land management in landslide-prone areas. This study used the GIS-AHP model to estimate the landslide susceptibility in Batang Kali, Selangor, Malaysia. The results showed that the most important factor was rainfall, followed by slope, soil moisture index, and aspect. The susceptibility map produced showed different high and very high susceptibility zones, especially in mountainous and heavily used areas. The ROC-AUC analysis for model validation showed an AUC value of 0.722, indicating adequate predictive performance and confirming the applicability of the AHP method for landslide susceptibility assessment at the regional level. The produced landslide susceptibility map provides helpful data to planners, engineers, and decision-makers to help reduce risk, plan infrastructure, and manage land use sustainably. The GIS-AHP approach is useful; however, this study has some limitations. Firstly, the data of soil and geology/lithology were not included in the influencing factors because of the difficulty of obtaining suitable and reliable spatial datasets for the study area. The exclusion of these factors may constrain the representation of subsurface conditions and their potential influence on landslide susceptibility. Secondly, the landslide inventory included 46 identified locations, which may not include all of the historical landslide cases in the study area. Therefore, the susceptibility results must be interpreted in light of the spatial and data limitations of the study. Future studies may involve further machine learning and clustering techniques to compare predicted performance and improve susceptibility evaluation in the study area.

Credit Authorship Contribution Statement

Marwa Sultan: Conceptualization, Methodology, Formal analysis, Investigation, Data curation, GIS analysis, Validation, Visualization, Writing – original draft. Siti Nur Aliaa Roslan: Supervision, Methodology, Writing – review & editing. Helmi Zulhaidi Mohd Shafri: Supervision, Writing – review & editing.

Declaration of Competing Interest

The authors declare that they have no known competing financial interests or personal relationships that could have appeared to influence the work reported in this paper.

REFERENCES

Abdo, H.G., 2025. Landslide susceptibility mapping in Al-Khawabi river basin, Tartous, Syria: An integrated approach of bivariate-statistical modelling and geospatial technology. *Environmental Challenges*, 21, Article 101327. https://doi.org/10.1016/j.envc.2025.101327

Abdulahi, M.M., Egli, P.E. and Bora, Z., 2026. Landslide susceptibility mapping in the Mount Elgon districts of Eastern Uganda using Google Earth Engine. *GeoHazards*, 7(2), Article 50. https://doi.org/10.3390/geohazards7020050

Abubakar, F., Abir, I.A. and Hassan, A.A., 2025. Kogi west geophysical mineralisation appraisal using Analytical Hierarchy Process (AHP). *Journal of African Earth Sciences*, 224, Article 105532. https://doi.org/10.1016/j.jafrearsci.2024.105532

Adamala, S., Velmurugan, A., Swarnam, T.P., Palakuru, M., Subramani, T., Jaisankar, I., Nanda, B.K., Kumari, N. and Srivastava, A., 2025. Soil moisture mapping in Indian tropical islands with C-band SAR and artificial neural network models. *Environmental Monitoring and Assessment*, 197(7), Article 758. https://doi.org/10.1007/s10661-025-14239-4

Addis, A., et al., 2024. Landslide susceptibility mapping using GIS and bivariate statistical models in Chemoga Watershed, Ethiopia. *Advances in Civil Engineering*, 2024, Article 6616269. https://doi.org/10.1155/2024/6616269

Adhikari, S. and Dhakal, S., 2026. Landslide susceptibility assessment and slope stability analysis of cut slopes along Dumre-Paudhi Bazar road section, western Nepal. *Geosystems and Geoenvironment*, 5(2), Article 100499. https://doi.org/10.1016/j.geogeo.2026.100499

Aguarón, J. and Moreno-Jiménez, J.M., 2003. The geometric consistency index: Approximated thresholds. *European Journal of Operational Research*, 147(1), pp. 137–145. https://doi.org/10.1016/S0377-2217(02)00255-2

Ait Omar, M., Etebaai, I., Taher, M. and Tawfik, A., 2025. Landslide susceptibility mapping in the Bokoya Massif, Northern Morocco: A geospatial and multi-factor analysis using the analytic hierarchy process (AHP). *Scientific African*, 30, Article e02980. https://doi.org/10.1016/j.sciaf.2025.e02980

Ali, A., Teku, D., Sisay, T. and Mihret, B., 2025. Geospatial modeling of landslide susceptibility in Debek, South Wollo, Ethiopia: comparative analysis of frequency ratio and analytical hierarchy process models for geohazards management. *Frontiers in Earth Science*, 13, Article 1557860. https://doi.org/10.3389/feart.2025.1557860

Al-Awadhi, T., Al Ramimi, W., Al Jabri, K. and Abulibdeh, A., 2025. Solar farms suitability analysis using GIS-Based Analytic Hierarchy Process (AHP) multi-criteria: a case study of Al Duqm – Oman. Renewable Energy, 241, Article 122295. https://doi.org/10.1016/j.renene.2024.122295

Al'Afif, M., Sartohadi, J. and Samodra, G., 2024. Impact of landslide on geoheritage: Opportunities through integration, geomorphological classification and machine learning. *International Journal of Geoheritage and Parks*, 12(2), pp. 333–351. https://doi.org/10.1016/j.ijgeop.2024.05.002

Badapalli, P.K., Gugulothu, S. and Nakkala, A.B., 2025. Geospatial and NDBI approaches for the Musi River basin morphometric studies in the metropolitan urban Cities of India. *Advances in Space Research*, 75(4), pp. 3375–3396. https://doi.org/10.1016/j.asr.2024.12.010

Bayable, G., Eshetie, G.G., Melese, T. and Melaku, A., 2025. Land use/cover classification using machine learning algorithms and their impacts on land surface temperature and soil moisture in the Alawuha Watershed, Ethiopia. *Environmental and Sustainability Indicators*, 27, Article 100797. https://doi.org/10.1016/j.indic.2025.100797

Bensalem, H., Besser, H., Amamria, S., Bensalem, M.S., Meisina, C. and Hamdi, N., 2026. Application of analytic hierarchy process (AHP) model for landslide susceptibility mapping in the Nouvelle Matmata region, southern Tunisia. *Journal of African Earth Sciences*, 242, Article 106237. https://doi.org/10.1016/j.jafrearsci.2026.106237

Chen, X., Li, W., Hsu, C.-Y., Arundel, S.T. and Higman, B., 2025. Harnessing geospatial artificial intelligence and deep learning for landslide inventory mapping: advances, challenges, and emerging directions. *Remote Sensing*, 17(11), Article 1856. https://doi.org/10.3390/rs17111856

Dai, X., Chen, J., Zhang, T. and Xue, C., 2025. Integrated landslide risk assessment via a landslide susceptibility model based on intelligent optimization algorithms. *Remote Sensing*, 17(3), Article 545. https://doi.org/10.3390/rs17030545

Das, D., Chattoraj, S.L. and Narayanan, S.A., 2026. Earth observation based landslide susceptibility mapping along the Kailash-Mansarovar route in Uttarakhand Himalaya using AHP-TOPSIS integrated approach. *Journal of Earth System Science*, 135(2), Article 103. https://doi.org/10.1007/s12040-026-02807-2

Ersayin, K., 2025. The influence of sampling strategies on shallow landslide susceptibility modelling in a mountainous area. *Landslides*, 23(2), pp. 531–546. https://doi.org/10.1007/s10346-025-02646-0

Gebrehiwot, A., Berhane, G., Kide, Y., Teklay, W., Mekonen, B. and Fissha, Y., 2025. Landslide susceptibility mapping in Lesalso (Laelay Maichew), Northern Ethiopia: a GIS approach using frequency ratio and analytical hierarchy process methods. *Modeling Earth Systems and Environment*, 11(6), Article 421. https://doi.org/10.1007/s40808-025-02578-7

Gacu, J., Kantoush, S., Candelario, R., Falculan, J., Moaje, K.V., Famaran, M.J., Nepomuceno, M., Ebon, J.A., Parungao, R., Ignacio, R., Merida, M., Pastrana, P.M. and Quinton, E., 2025. Integrated multi-hazard risk assessment under compound disasters using analytical hierarchy process (AHP). *Heliyon*, 11(11), Article e43173. https://doi.org/10.1016/j.heliyon.2025.e43173

Ghosh, K. and Saha, R., 2025. A critical review on rainfall induced landslide occurrences and early warning systems. *Geomechanics and Geoengineering*, 20(5), pp. 1052–1074. https://doi.org/10.1080/17486025.2025.2496302

Ishak, N.M., Khan, A., Abdullah, J., Salleh, S.A. and Santamouris, M., 2025. Optimizing seasonal performance of advanced heat mitigation solutions for city-scale thermal management in Greater Kuala Lumpur. *City and Environment Interactions*, 28, Article 100219. https://doi.org/10.1016/j.cacint.2025.100219

Kara, C. and Iranmanesh, A., 2025. Protection boundary development in historical–cultural built environments using Analytical Hierarchy Process (AHP) and Geographic Information System (GIS). *Urban Science*, 9(5), Article 173. https://doi.org/10.3390/urbansci9050173

Kashyap, A. and Behera, M.D., 2023. Geomorphic response of bedrock landslides induced landscape evolution across the Teesta catchment, Eastern Himalaya. *Environmental Earth Sciences*, 82(8), Article 193. https://doi.org/10.1007/s12665-023-10859-6

Khan, S., Siddique, T., Haris, P.M., Gupta, K., Ahamad, A. and Mondal, M.E.A., 2026. Comparative landslide susceptibility mapping along national highway 109 using analytical hierarchy process and frequency ratio method. *Discover Geoscience*, 4(1), Article 89. https://doi.org/10.1007/s44288-026-00456-y

Kozák, M. and Šilhán, K., 2023. Contrasting landslide activity on slopes with different structural geology: evidence from dendrogeomorphic analysis. *Landslides*, 20(9), pp. 1893–1903. https://doi.org/10.1007/s10346-023-02067-x

Kucuker, D.M., 2025. Analyzing landslide susceptibility of forest roads by analytical hierarchy process

(AHP) in Of forest planning unit of Turkiye. *Natural Hazards*, 121(2), pp. 2323–2345. https://doi.org/10.1007/s11069-024-06882-w

Kumar, A., Kanga, S., Choudhury, U., Singh, S.K., Rana, R.S., Meraj, G. and Kumar, P., 2025. Landslide susceptibility mapping using statistical information value model: a case study of part of Chamoli District, Uttarakhand India. *Risk Analysis*, 45(12), pp. 4726–4742. https://doi.org/10.1111/risa.70141

Lai, J. and Qi, S., 2026. Landslide susceptibility prediction and driving force analysis integrating machine learning and spatial factor optimization: a case study in the Guanyinyan Hydropower Station Reservoir Area. *Land Degradation & Development*, 37(8), pp. 3609–3627. https://doi.org/10.1002/ldr.70331

Lee, S., Roh, M., Jo, H.-W., Joon, K. and Lee, W.-K., 2025. Machine learning-based rainfall-induced landslide susceptibility model and short-term early warning assessment in South Korea. *Landslides*, 22(8), pp. 2809–2827. https://doi.org/10.1007/s10346-025-02513-y

Liu, S., Wang, L., Zhang, W., He, Y. and Samui, P., 2023. A comprehensive review of machine learning-based methods in landslide susceptibility mapping. *Geological Journal*, 58(6), pp. 2283–2301. https://doi.org/10.1002/gj.4666

Liu, Y., Han, X., Cui, X., Li, X. and Jin, H., 2025. Spatial heterogeneity of landslide distribution and its drivers in the Yangtze River Basin: a remote sensing and GIS-based multi-factor analysis. *Frontiers in Environmental Science*, 13, Article 1576700. https://doi.org/10.3389/fenvs.2025.1576700

Lusiana, N., Adliya, G.E., Devianto, L.A. and Husin, N.A., 2026. Rapid post-landslide vegetation regrowth detected by multi-temporal satellite imagery in the Southern part of Mt. Rinjani National Park, Lombok, Indonesia. *Natural Hazards*, 122(5), Article 191. https://doi.org/10.1007/s11069-025-07964-z

Lv, Z., Wang, S., Yan, S., Han, J. and Zhang, G., 2024. Landslide susceptibility assessment based on multisource remote sensing considering inventory quality and modeling. *Sustainability*, 16(19), Article 8466. https://doi.org/10.3390/su16198466

Machireddy, S.R., 2025. Geospatial technology approach for soil moisture estimation in Kurnool District, Andhra Pradesh, using NDVI and LST. *Sensing and Imaging*, 26(1), Article 62. https://doi.org/10.1007/s11220-025-00598-2

Mao, Y., Zhu, L., Chen, J. and Nanehkaran, Y.A., 2025. Adaptive modeling of landslide susceptibility using Analytical Hierarchy Process and Multi-Objective Decision Optimization. *Advances in Space Research*, 75(6), pp. 4536–4551. https://doi.org/10.1016/j.asr.2024.12.061

Martin, B., Bennett, T.D., DeWitt, P.E., Russell, S. and Sanchez-Pinto, L.N., 2025. Use of the area under the precision–recall curve to evaluate prediction models of rare critical illness events. *Pediatric Critical Care Medicine*, 26(6), pp. e855–e859. https://doi.org/10.1097/PCC.0000000000003752

Mohd Noh, M.R., Rosle, Q.A., Tuan Mohamed, T.R.T., Ahmad, F., Harun, A.R. and Ramli, Z., 2024. Geological factors contributing to landslide incident in Malaysia: case study Batang Kali landslide disaster, Hulu Selangor, Selangor. *Thai Geoscience Journal*, 5(8), pp. 34–44. https://doi.org/10.14456/tgj.2024.5

Öztürk, Ş., 2025. Comparative landslide susceptibility mapping using local inventories: a case study from Trabzon, Türkiye. *Natural Hazards*, 121(12), pp. 14655–14676. https://doi.org/10.1007/s11069-025-07371-4

Panchal, S. and Srivastava, A.K., 2026. GIS-based landslide susceptibility mapping of Almora District in India: a comparison of different techniques. *Geological Journal*, 61(3), pp. 671–687. https://doi.org/10.1002/gj.70002

Pawar, N.S. and Sharma, K.V., 2025. Comprehensive review of remote sensing integration with deep learning in landslide forecasting and future directions. *Natural Hazards*, 121(20), pp. 23687–23721. https://doi.org/10.1007/s11069-025-07171-w

Pei, Y., Qiu, H., Zhu, Y., Wang, J., Yang, D., Tang, B., Wang, F. and Cao, M., 2023. Elevation dependence of landslide activity induced by climate change in the eastern Pamirs. *Landslides*, 20(6), pp. 1115–1133. https://doi.org/10.1007/s10346-023-02030-w

Petley, D., 2023. The official report into the 16 December 2022 Batang Kali landslide. *Eos, The Landslide Blog*, 23 October. https://eos.org/thelandslideblog/batang-kali-landslide-1 (Accessed: 5 September 2026).

Pramanik, M. and Hegde, A., 2026. Assessing future landslide susceptibility and risk escalations under changing LULC and climate conditions in the Western Ghats of Karnataka in India. *Scientific Reports*, 16, Article 16963. https://doi.org/10.1038/s41598-026-47255-6

Punyal, S. and Kumar, D.P., 2026. Using the topographic wetness index (TWI) to identify landslide risks to rural water supplies and sanitation in the Indian Himalayan. *International Journal of Aquatic Research and Environmental Studies*, 6(S1), pp. 384–395. https://www.injoere.com/index.php/injoere/article/view/758

Qiu, H. and Wei, Y., 2025. Landslide geomorphology: pattern, process and stability. *Journal of Earth Science*, 36(1), pp. 327–332. https://doi.org/10.1007/s12583-024-0131-z

Ramdani, R.S., Fehdi, C., Gueraidia, N.E.H., Gueraidia, S. and Hafnaoui, S., 2025. Remote sensing-based assessment of natural hazard susceptibility in the Safsaf watershed, Northeast Algeria. *International Journal of Energy and Water Resources*, 9(4), pp. 2719–2726. https://doi.org/10.1007/s42108-025-00416-1

Reichenbach, P., Rossi, M., Malamud, B.D., Mihir, M. and Guzzetti, F., 2018. A review of statistically-based landslide susceptibility models. *Earth-Science Reviews*, 180, pp. 60–91. https://doi.org/10.1016/j.earscirev.2018.03.001

Riesthuis, P. and Otgaar, H., 2025. On the use of receiver operating characteristic area under the curve in eyewitness memory research. *Legal and Criminological Psychology*, 30(2), pp. 212–230. https://doi.org/10.1111/lcrp.12300

Ružek, I. and Šilhán, K., 2024. Regional activity of landslide movements affecting the bank of meandering river: insights using tree-ring based methods. *CATENA*, 242, Article 108141. https://doi.org/10.1016/j.catena.2024.108141

Saaty, T.L., 1977. A scaling method for priorities in hierarchical structures. *Journal of Mathematical Psychology*, 15(3), pp. 234–281. https://doi.org/10.1016/0022-2496(77)90033-5

Saaty, T.L., 2003. Decision-making with the AHP: why is the principal eigenvector necessary. *European Journal of Operational Research*, 145(1), pp. 85–91. https://doi.org/10.1016/S0377-2217(02)00227-8

Selamat, S.N., Abd Majid, N. and Mohd Taib, A., 2023. A comparative assessment of sampling ratios using artificial neural network (ANN) for landslide predictive model in Langat River Basin, Selangor, Malaysia. *Sustainability*, 15(1), Article 861. https://doi.org/10.3390/su15010861

Sharma, N., Saharia, M. and Ramana, G.V., 2024. High resolution landslide susceptibility mapping using ensemble machine learning and geospatial big data. *CATENA*, 235, Article 107653. https://doi.org/10.1016/j.catena.2023.107653

Sujatha, E.R. and Sudharsan, J.S., 2024. Landslide susceptibility mapping methods—a review. In: Panda, G.K., Shaw, R., Pal, S.C., Chatterjee, U. and Saha, A. (eds.), *Landslide: Susceptibility, Risk Assessment and Sustainability: Application of Geostatistical and Geospatial Modeling*. Advances in Natural and Technological Hazards Research, 52. Springer, Cham, pp. 87–102. https://doi.org/10.1007/978-3-031-56591-5_4

Tukku, M.A., Karuppannan, S., Meten, M., Garo, T. and Fekadu, A., 2025. Landslide susceptibility modeling in West Shoa Zone, Central Ethiopia: an integrated geospatial and statistical analysis. *Scientific African*, 28, Article e02772. https://doi.org/10.1016/j.sciaf.2025.e02772

Wang, X.-M., Xu, Y.-F. and Liu, L.-L., 2026. Automated unsupervised landslide detection in infrastructure-exposed mountainous regions using Sentinel-2 NDVI time-series analysis. *Automation in Construction*, 187, Article 106967. https://doi.org/10.1016/j.autcon.2026.106967

Woldesenbet, T.T., Arefaine, H.B. and Yesuf, M.B., 2023. Numerical stability analysis and geotechnical investigation of landslide prone area (the case of Gechi district, Western Ethiopia). *Environmental Challenges*, 13, Article 100762. https://doi.org/10.1016/j.envc.2023.100762

Wood, N.J. and Jones, J.M., 2025. Variations in road exposure and traffic volumes in the United States in areas susceptible to landslides. *International Journal of Disaster Risk Reduction*, 124, Article 105567. https://doi.org/10.1016/j.ijdrr.2025.105567

Xian, Y. and Wei, X., 2025. Failure mechanism of a snowmelt-related loess landslide group in Ten-zan, China. *Geoenvironmental Disasters*, 12(1), Article 30. https://doi.org/10.1186/s40677-025-00334-8

Zhao, B., Zhu, J., Hu, Y., Liu, Q. and Liu, Y., 2022. Mapping landslide sensitivity based on machine learning: a case study in Ankang City, Shaanxi Province, China. *Geofluids*, 2022, Article 2058442. https://doi.org/10.1155/2022/2058442

Zhou, Q., Luo, Y., Shi, C. and Li, Y., 2023. Hydrological effects of vegetation restoration in karst areas research: progress and challenges. *Transactions in Earth, Environment, and Sustainability*, 1(2–3), pp. 177–204. https://doi.org/10.1177/2754124X231199565

Zighmi, K., Zahri, F., Faqeih, K., Al Amri, A., Riheb, H., Alamri, S.M. and Alamery, E., 2025. AHP multi criteria analysis for landslide susceptibility mapping in the Tellian Atlas chain. *Scientific Reports*, 15, Article 25747. https://doi.org/10.1038/s41598-025-10819-z

رسم خرائط قابلية حدوث الانهيارات الأرضية باستخدام نظم المعلومات الجغرافية وعملية التحليل الهرمي (AHP) في باتانغ كالي، سيلانغور، ماليزيا

مروى سلطان عبد العتبي[1،*]، سيتي نور عليا رسلان[1]، حلمي زولهيدي مهدي شافري[2،1]

قسم الهندسة المدنية، كلية الهندسة، جامعة بوترا الماليزية، سيردانك، ماليزيا[1]

مركز أبحاث علوم المعلومات الجغرافية المكانية، كلية الهندسة، جامعة بوترا الماليزية، سيردانك، ماليزيا[2]

خلاصة

تُعدّ الانهيارات الأرضية من المخاطر البيئية الشائعة في ماليزيا، حيث تحدث بشكل رئيسي في المناطق الجبلية والاستوائية، وغالبًا خلال فترات هطول الأمطار الغزيرة. تهدف هذه الدراسة إلى تقييم قابلية حدوث الانهيارات الأرضية في باتانغ كالي، سيلانغور، ماليزيا، باستخدام عملية التحليل الهرمي (AHP) القائمة على نظم المعلومات الجغرافية (GIS). استنادًا إلى السجلات التاريخية، وتفسير الصور الجوية، وبيانات الاستشعار عن بُعد، بالإضافة إلى التحقق الميداني، تم إنشاء قاعدة بيانات للانهيارات الأرضية تضم 46 موقعًا محددًا للانهيارات الأرضية. تم اختيار ستة عشر عاملًا مؤثرًا، تشمل عوامل طبوغرافية وهيدرولوجية وبيئية وبشرية متنوعة، لنمذجة قابلية حدوث الانهيارات الأرضية. تم إنشاء خريطة قابلية حدوث الانهيارات الأرضية باستخدام تحليل التراكب الموزون، وصُنّفت إلى خمسة مستويات من القابلية، تتراوح من منخفضة جدًا إلى عالية جدًا. تُظهر خريطة قابلية حدوث الانهيارات الأرضية الناتجة أن 14.68% من منطقة الدراسة تقع ضمن فئة القابلية المنخفضة جدًا للانزلاق، بينما تقع 25.84% و20.20% و24.90% و14.38% ضمن فئات القابلية المنخفضة، والمتوسطة، والعالية، والعالية جدًا للانزلاق على التوالي. تُعدّ خريطة قابلية حدوث الانهيارات الأرضية الناتجة عن هذه الدراسة أداةً واقعية لدعم اتخاذ القرار للحدّ من مخاطر الانهيارات الأرضية، وتصميم البنية التحتية، وتعزيز الإدارة المستدامة للأراضي في المناطق الجبلية الحساسة. أُجري تحليل منحنى خصائص تشغيل المستقبل (ROC) لقياس الأداء التنبؤي للنموذج، باستخدام المساحة تحت المنحنى (AUC) كمقياس شامل لتمييز النموذج. أظهر تحليل ROC–AUC قيمة AUC قدرها 0.722 (72.2%)، مما يُشير إلى أداء مقبول للنموذج.

الكلمات المفتاحية: عملية التحليل الهرمي (AHP)، المساحة تحت المنحنى (AUC)، نظم المعلومات الجغرافية، رسم خرائط قابلية حدوث الانهيارات الأرضية، الاستشعار عن بُعد.